Received: Date Month Year | Revised: Date Month Year | Accepted: Date Month Year

DOI: xxx

RESEARCH ARTICLE

Highly integrated transmitting and receiving Phased Array with multi-channels and high efficiency in K/Ka-Band SatCom application

Qiaoshan Zhang[1, 2] | Xiaowei Shi[1] | Steven Gao[3] | Yan Li[2] | Qi Luo[4] | Jixiang Wan[2] | Zhaoxuan Xue[2] | Lehu Wen[3]

[1]School of Electronic Engineering, Xidian University, Xi'an, China

[2]Department of Antenna Engineering, Xi'an Institute of Space Radio Technology, Xi'an, China.

[3]School of Engineering and Digital Arts, University of Kent, U.K.

[4]School of Physics, Engineering and Computer Science, University of Hertfordshire, Hatfield, U.K.

Correspondence

Qiaoshan Zhang, School of Electronic Engineering, Xidian University, Xi'an, 710071, China.

Email: zhangqs_504@163.com

Funding information

China Scholarship Council;

EPSRC, Grant/Award Number: EP/N032497/1; EP/S005625/1.

Abstract

A highly integrated K/Ka-band phased array with duplexing channels for transmitting and dual circularly polarized channels for receiving is presented. To increase both the efficiency and channel isolation, a novel architecture is proposed to integrate the horn antenna, polarizer, ortho-mode transducer (OMT), and filters within a very compact radiating aperture as the element. Based on this element, one large-scale phased array with 416 elements was developed, fabricated, and measured. Experimental results show that the proposed phased array has high aperture efficiency of larger than 56% in both transmitting and receiving channels, high channel isolations of 50dB between different frequency channels and 20dB between different polarization channels. Furthermore, beam scanning performance within ±20º and ±18º at 20 GHz and 30 GHz are achieved, respectively. The developed multifunctional phased array is an attractive and feasible frontend for K-/Ka- band Satcom system.

KEYWORDS

Satellite phased array, dual-band, multi-channel, high channel isolation.

1 INTRODUCTION

With flexible beam scanning ability, active phased array antennas (APAAs) are promising radio frontends for the next generation of satellite payloads.[1] Up to date, most of existing spaceborne APAAs are designed in single frequency band, and two phased arrays are typically used for the transmitting (Tx) and receiving (Rx), respectively.[2, 3] To increase the system capacity, a phased array with two separated frequency bands for Tx/Rx functions in the same aperture has become the latest research trend. However, due to the issues such as electromagnetic compatibility (EMC), fabrication difficulty and heat dissipation caused by integration, the implementation of a dual-band phased array on the satellite is a challenging task.

Recently, several methods are presented to realize a dual-band array antenna design, including interleaving or overlapping elements of different frequencies,[4,5] using element with multi-resonant modes,[6] using wideband element.[7] Due to the advantages of low cost, low profile and easy fabrication, most of the antenna arrays reported in the literature use the microstrip radiator and microstrip beamforming networks.[4-9] However, microstrip-type phased arrays have inherent

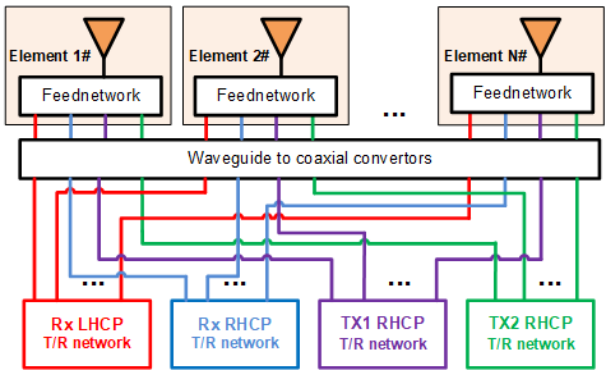

FIGURE 1 Architecture of the proposed four-channel phased array.

drawbacks of high loss, narrow bandwidth and low channel isolation. In[10, 11], horn antennas are introduced as the radiators for satellite array antenna. Although a horn with a conical helix inside is employed in[11] to obtain a dual-band phased array with separated signal channels, it suffers from small scanning range and low aperture efficiency due to the large element space and high loss caused by the bulky unit cell.

In this article, a novel architecture of highly integrated phased array is developed for K-/Ka- band satellite applications, as shown in Figure 1. It is used to solve the great challenging work of a phased array to obtain dual-band operations at transmitting end and dual-circular-polarization operations at receiving end. In order to minimize the loss and simplify the design of beam-forming network, a novel configuration of the array element is designed in the waveguide-type, integrating the horn antenna, Ortho-mode transducer (OMT), polarizer, and filters into a very compact aperture with four well-isolated channels. Simulated and experimental results show that the presented multifunctional phased array can scan the beams in the ranges of ±20º and ±18º in the K- and Ka-band, respectively. The aperture efficiency of larger than 56%, operating bandwidth of wider than 2GHz and channel isolation of larger than 20dB are achieved in both bands by the presented phased array, showing competitive performance than other reported work. Moreover, with the power handling capacity and space environmental adaptability, the proposed phased array can be an attractive candidate for satellite application.

TABLE I Electrical Requirements of the Phased Array

Channel	BW(GHz)	Polarization	Gain (dBi)	SLL (dB)
Tx	19~21	LHCP	≥38 @20 GHz	≤-10
Rx	29~31	LHCP&RHCP	≥40.5 @30GHz	
Channel	**Isolation (dB)**		**VSWR**	**Coverage**
Tx	≥50	≥60 (Tx & Rx)	≤ 1.3	-10º≦θ≦10º
Rx	≥20			0º≦φ≦180º

2 Unit cell Design and Verification

The phased array in this work is designed for a K/Ka bands satellite communication (Satcom) payload, which is defined by the Electronic Communications Committee (ECC).[12] The detailed requirements are listed in Table I. It can be seen that stringent specifications of high aperture efficiency and high channel isolation at both bands are required. In order to meet the above requirements, horn antenna with integrated waveguide feed network is employed as the unit cell. However, the high integration of four waveguide channels in K-/Ka- band is challenging for the limitation of the array spacing. Although the state-of-the-art compact Ka-band feed network in[13] has a horizontal diameter of 33 mm^2 ($3.3\lambda_0$), which is too large to apply in a phased array. Thus, a new structure is proposed with the horizontal dimension of less than 23 mm^2 in our work, as shown in Figure 2. It consists of a horn antenna, a polarizer, a combined orthogonal-mode transducer (OMT), a Tx filter, a Tx diplexer and two Rx filters. In spite of only single circular polarization is applied in Tx band, two sub-frequency-band channels for Tx signals are provided by the diplexer to improve the system functionality.

Hexagonal-shaped short-circular-ring horn antenna is applied in our design as its advantages of high

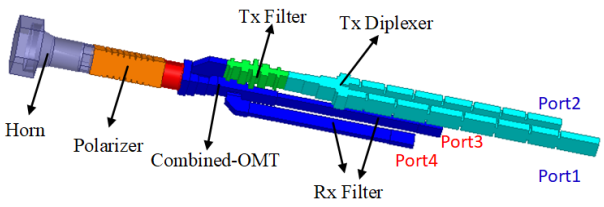

FIGURE 2 Configuration of the proposed element.

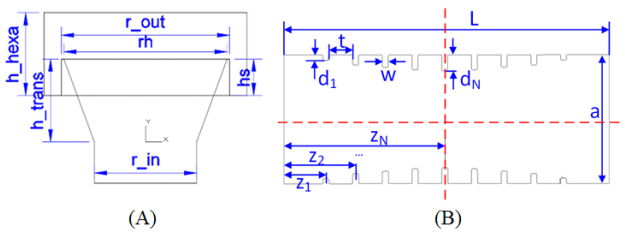

FIGURE 3 Layout of the designed A, horn. (r_in=6.2, rh=9.9, r_out=10, hs=4.4, h_hexa=10, h_trans=10). B, polarizer. (a=10.8, w=0.5, t=2, L=30, d1=0.45, d2=0.85, d3=1.05, d4=1.25, d5=1.35, Z1=5, Z2=7.5, Z3=10, Z4=12.5, Z5=15). (Unit: mm).

efficiency, low profile, and easy fabrication. Moreover, array with this horn can make full use of the aperture in a hexagonal lattice, and then maximize the entire array's aperture efficiency. The configuration of the horn antenna is shown in Figure 3A. This horn is designed to operate at higher-order modes (TM_{11}, TE_{21}) on the aperture caused by the gap between the inner cylinder and the outer hexagonal boundary, which reduces the cross-polarization level and improves the radiation efficiency. The geometrical parameters *rh* and *hs* determine the gain of the horn, and then can be used to optimize the gain performance in both bands.

The wideband dual circular polarization function of the unit cell is realized by using a square corrugated waveguide polarizer with low axial ratio and low reflection coefficient in both bands. The designed polarizer and its geometrical parameters are shown in Figure 3B. To reduce the length of the conventional waveguide polarizer[14], fewer irises are used through enlarging the iris interval and fixing the initial iris heights d(n) by the linear taper, as defined in Equation

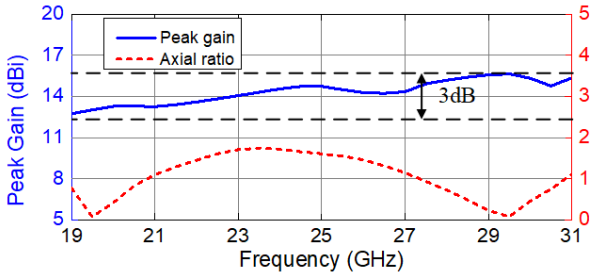

FIGURE 4 Simulated peak gain and Axial ratio of the horn and polarizer.

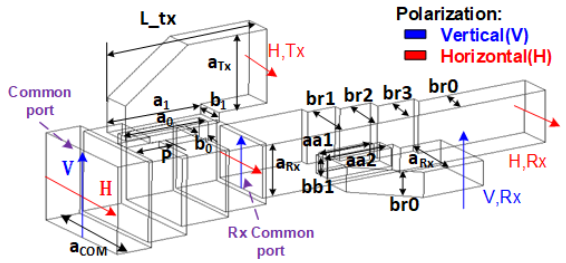

FIGURE 5 The proposed dual-band combined-OMT with dual-polarization in Rx band. acom=10.4, aRx=6.2, a0=7.65, b0=1.25, a1=8.8, b1=2.6, P=4.4, L_tx=13.3, aTx=8.8, br1=5.4, br2=4.7, br3=3.7, br0=3, aa1=4.8, aa2=5.95, bb1=2.2. (Unit: mm)

1, thus, wide axial ratio bandwidth is achieved.

$$d(n) = d_1 + \frac{2(d_N - d_1)}{L} \times Z(n) \qquad (1)$$

Commercial full-wave electromagnetic software Ansys HFSS is used for antenna design. The horn and polarizer are co-designed and simulated for evaluating the circularly polarized radiation performance, and the results are shown in Figure 4. It can be seen that the 3dB-gain bandwidth covers the entire frequency band from Tx to Rx, and the simulated AR is lower than 1 dB in both the Tx band and Rx band.

Compared to the conventional OMT[15], a new compact combined-OMT is developed in this work to divide three different channels, including Tx channel, horizontal and vertical polarized Rx channels. The configuration and ports definition of the OMT are shown in Figure 5 with the geometrical parameters given in the Figure caption. To reduce the profile, the square transition section and a narrow gap coupling window are innovatively designed to transmit the Tx signals through the window and receive the dual-polarized Rx signals through the straight square waveguide port. Therefore, the square transition can be seen as a high-pass filter also. To assure efficient transmission in the OMT for both Tx and Rx signals, the sizes of the square waveguides *acom* and *aRx* are designed to only pass the dominate modes in corresponding frequency bands. Moreover, the value of a_{com} is related to suppress the propagation of the

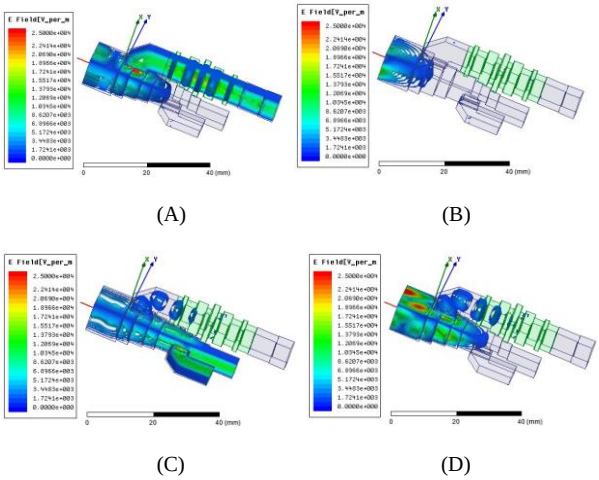

(A) (B)

(C) (D)

FIGURE 6 Electric-field distributions in the combined-OMT and Tx filter. A, Dominant mode excited in common port @ 20GHz. B, Higher order modes excited in common port @ 20GHz. C, Dominant mode excited in common port @ 30GHz. D, Higher order modes excited in common port @ 30GHz.

TE_{12} mode and other higher order modes for the Rx signals. By optimizing the sizes of square waveguide steps, position of the coupling window, and Tx filter position, the proposed OMT is matched in both bands without using any traditional matching methods such as the use of thin septum, pins, and thin irises. As a result, machining complexity is significantly reduced.

The electric field distributions of the matched OMT and Tx filter is shown in Figure 6. The model is excited by dominate modes and other higher order modes including the TE_{11}, TM_{11}, TE_{20}, TE_{02}, TE_{21}, TE_{12} in common port in the center frequency of both Tx and Rx bands. As can be seen in Figure 6A, the dominate modes of 20GHz pass through the Tx channel but will be rejected by the Rx channels. As shown in Figure 6B, the higher order modes of 20GHz are rejected by both Tx and Rx channels, so it cannot be excited and transmitted in the proposed feed network. Similarly, in Figure 6C and Figure 6D, the dominate modes of 30GHz can only pass through the Rx channels, while the higher order modes cannot be excited and transmitted in the feed network. It can be concluded that highly efficient transmission and no

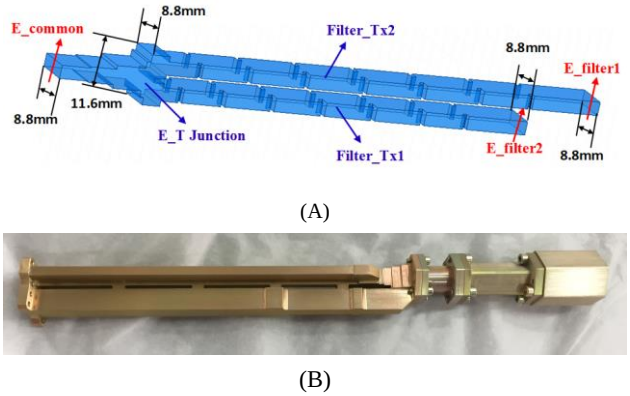

(A)

(B)

FIGURE 7 A, Configuration of the proposed diplexer. B, Prototype of the proposed radiating element

deterioration on the radiating pattern by higher order modes can be obtained for the element.

The diplexer is used to divide the Tx channel of the OMT into two sub-band channels, which employs septate E-plane waveguide with two iris-typed band-pass waveguide filters, as shown in Figure 7A. Compared to Y-junction, T-junction and other structures[16], the designed diplexer is more compact in the horizontal dimension. Because the directions of the electric fields in the structure are always identical, higher-order modes can be efficiently suppressed. The filters in the diplexer utilize multiple resonant cavities to obtain a fast roll-off rate at the band-edge. Therefore, the high channel isolation between two sub bands is obtained with an extremely narrow band gap.

Figure 7B shows the fabricated prototype of the element. Its dimension is only 22.3mm×25.75 mm×265mm and weight is 85g. The S-parameters were measured by Agilent N5244A vector network analyzer. The simulated and measured results at the four ports in the Tx and Rx bands are compared in Figure 8A and Figure 8B. The slight inconsistency is caused by the measurement and fabrication errors. Experimental results show that the reflection coefficients are lower than -15 dB in the required Tx and Rx bands. The measured isolations are better than 50 dB between Tx ports and 20 dB between Rx ports. The isolations between the Tx and Rx ports with the same polarization are higher than 100dB in Tx band and 80dB in Rx band. Both the simulated and measured radiation patterns of the array element at 20GHz and 30GHz are shown in Figure 8C and Figure

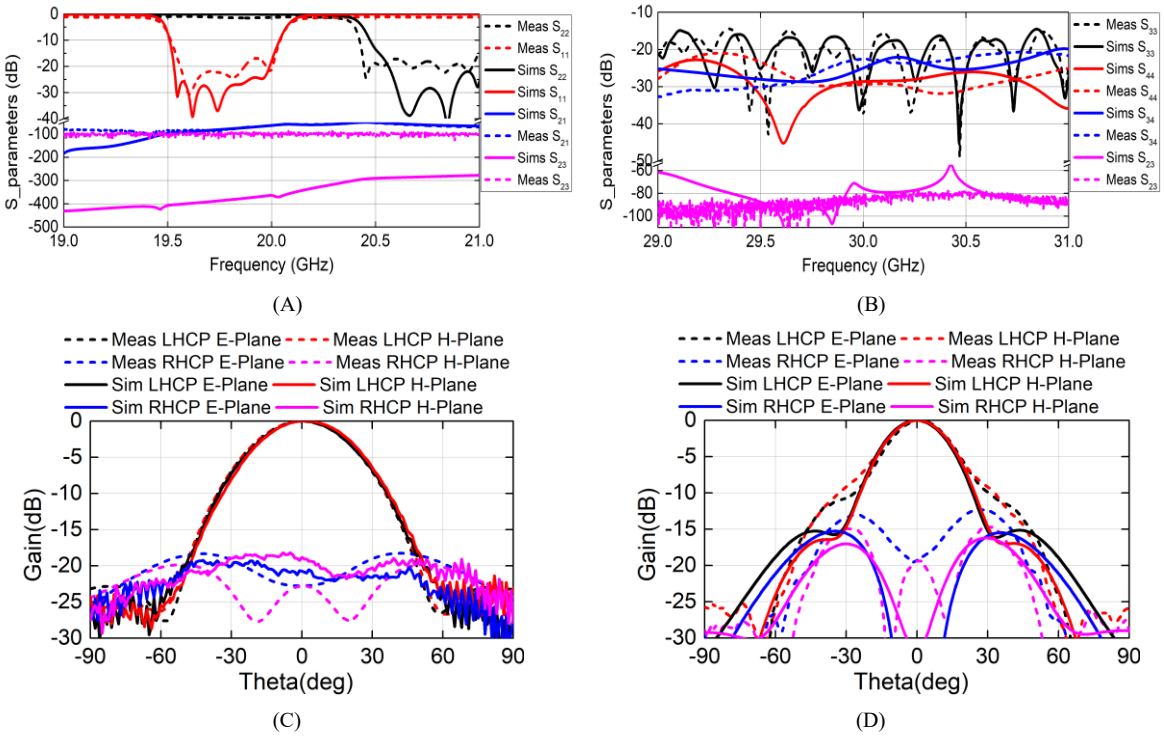

FIGURE 9 Simulated and measured results of the proposed Element. A, S-parameters in Tx band. B, S-parameters in Rx band. C, radiation patterns @20GHz and D, radiation patterns @30GHz.

8D. Good agreements can be observed in the main beam region especially at 20 GHz. The measured peak gains are 12.6 dBi and 15.4 dBi at 20GHz and 30GHz, corresponding to element efficiencies of 82.9% and 70.2%, respectively.

3 Array design, fabrication, and measurement

A phased array with 416 elements in a hexagonal lattice is designed to form a 20×24 cross aperture. The array factor is:

$$F(\theta,\varphi)=1+\sum_{m=-\left(\frac{M}{2}-1\right)}^{\frac{M}{2}-1}\sum_{n=-\left(\frac{N}{2}-1\right)}^{\frac{N}{2}-1} I_{mn}e^{jkd(\theta,\varphi)} \qquad (2)$$

$$d(\theta,\varphi)=(md_x+nd_x)sin\theta cos\varphi - md_x sin\theta_{mn}\cos\varphi_{mn} - nd_y sin\theta_{mn}\sin\varphi_{mn} \qquad (3)$$

where I_{mn}, θ_{mn} *and* φ_{mn} are the amplitude and the phase shift of the (m, n) element compared to the center element in the array.

To efficiently evaluate the deterioration of radiation and isolation caused by the mutual coupling, a seven-element array is simulated. Figure 10 show the scanning normalized radiation patterns along the E-plane at 20 GHz and 30 GHz, and the simulated results are summarized in Table II. It can be seen that beam scanning ranges with side-lobe level lower than -10 dB and gain fluctuation lower than 3 dB are ±20º at 20 GHz and ±18º at 30 GHz. Regarding the mutual

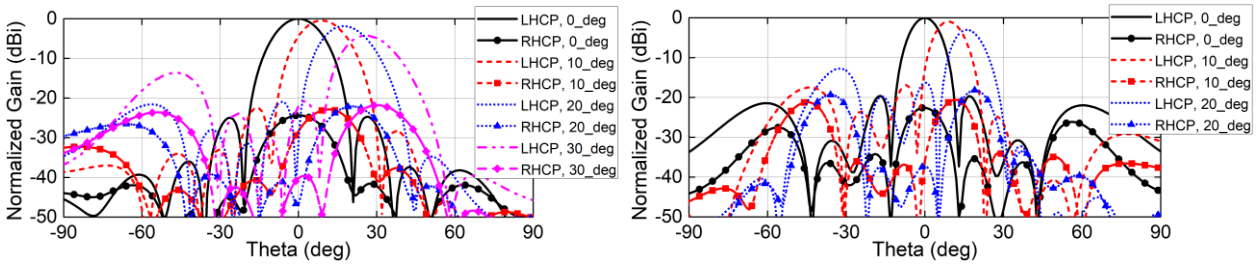

FIGURE 10 Simulated and measured radiation patterns of the proposed Element A, 20GHz and B, 30GHz.

TABLE II

SUMMARY OF PERFORMANCE OF THE DESIGNED SEVEN-ELEMENT ARRAY

ITEM	Frequency	0deg	10deg	20deg	30deg
Peak Gain	20 GHz	20.61	20.24	18.79	16.43
(dBi)	30 GHz	23.49	22.6	19.65	/
Side-lobe	20 GHz	24.93	22	19.69	9.38
lever (dB)	30 GHz	19.58	15.97	7.63	/
Active S_{11}	20 GHz	<-14.5	/	/	/
(dB)	30 GHz	<-21	/	/	/
Isolation	20 GHz	Tx_F1 / Tx_F2: >50; Tx / Rx: >60			
(dB)	30 GHz	Rx1 / Rx2: >20; Tx / Rx: >60			

coupling, the active S_{11} of center element for both Tx and Rx ports are analyzed. The results show that there is no significant difference compared to the passive S_{11} of the single element. Moreover, the isolations between different ports of the center element in Tx and Rx band are consistent with that of the single element. Therefore, the suppression of the mutual coupling has been proved.

To fulfill the gain requirement given in Table I, a prototype with 416 elements was fabricated and measured. The horns were fabricated side by side in a whole aluminum alloy plate. Other components are manufactured separately and then assembled using the flanges. The elements are connected to the T/R networks by the cables and SMP connectors. Figure 11 show the photos of the assembled prototype, whose dimension is 462 mm×462 mm×400 mm.

The radiation patterns of the prototype were measured in a far-field anechoic chamber with the elements excited in Taylor distribution in amplitude. Due to the availability of the T/R network, only the radiation patterns at 30GHz band was measured. The

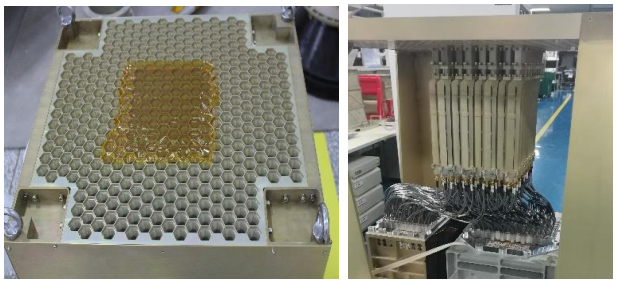

(A) (B)

FIGURE 11 Array prototype with 416 elements. A, Top view. B, Side view.

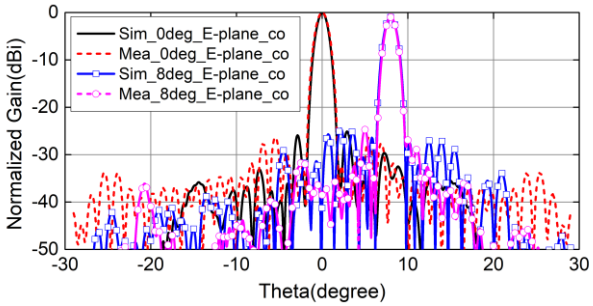

FIGURE 12 Measured and Simulated E-plane radiation patterns of the prototype at 30GHz when the main beams focus on 0º and 8º.

simulated and measured results are compared in Figure 12 when the main beam scans to 0º and 8º. Good agreements are achieved, especially in the main lobe region. The measured gain without the loss of the T/R network is 40.68dBi, corresponding to an aperture efficiency of 56.9%. Compared to the result of 58% of the seven-element array, the scaling of the array can be easily performed with little deterioration on the radiation performance. Besides, the measured SLLs are lower than -25 dB and -24 dB for the main beam scanning at 0º and 8º, respectively.

To the best knowledge of the authors, the proposed work is the first implementation of the multifunctional phased array in K/Ka- band with four channels. Table III lists the comparisons between the presented phased array with recently reported beam-steering arrays. It can be concluded that competitive performances of

TABLE III

COMPARISON WITH OTHER DUAL-BAND PHASED ARRAYS

Ref.	Operation bands (GHz)	N	Isolation (dB)	Aperture Efficiency	Scan range
[9]	F1: 20.35-21.15 F2: 30.08-30.88	2	F1: >15 F2: >10	F1: 25% F2: 7%	±5º
[17]	F1: 1.21-1.29 F2: 9.5-9.8	4	F1: >20 F2: >20	F1: 50% F2: 50%	±20º
[18]	F1: 14-17 F2: 33.8-35.3	2	F1: >25 F2: >70	F1: 68.8% F2: 36.7%	±40º
[19]	F1: 5.25-5.7 F2: 9.4-10	4	F1: >25 F2: >35	F1: 59.4% F2: 55.6%	±15º
This work	F1: 19-21 F2: 29-31	4	F1: >50 F2: >20	F1: 71% F2: 56.9%	±20º

N means the number of channels.

impedance bandwidth, radiation efficiency, and channel isolation are obtained by the presented work.

4 Conclusion

In this article, a novel K/Ka- band phased array based on elementary hexagonal horn and waveguide feed network is developed. The presented array shows high efficiency and high channel isolation. A new compact structure for the feed network is developed to integrate four channels of different sub-frequency bands in K-band and different polarizations in Ka-band. The phased array is designed, fabricated and measured. The comparison of the simulation and measurement shows good agreement. With promising performance in aperture efficiency, beam-scanning ability, channel isolation, power handling capacity and environmental adaptability, the proposed dual-band phased array can be a good candidate for satellite applications.

REFERENCES

1. W. A. Imbriale, S. Gao, and L. Boccia, Space Antenna Handbook. Chichester, West Sussex, U.K.: Wiley, 2012.
2. I. Chiba, Y. Konishi and T. Nishion, “Progress of Phased Array Systems in Japan,” 2010 IEEE International Symposium on Phased Array Systems and Technology, 19-28 Oct, 2010.
3. P.Capece, P.Carati, S.Contu, D. Maiarelli, R. Mizzoni, P.Noschese, R.Trento, P.Valle, “Array Technology in Thales Alenia Space Italia,” 3rd European Conference on Antennas and Propagation, 2009.
4. A.-I. Sandhu, E. Arnieri, G. Amendola, L. Boccia, E. Meniconi, and V. Ziegler, “Radiating Elements for Shared Aperture Tx/Rx Phased Arrays at K/Ka Band,” IEEE Trans. Antennas Propag., Vol. 64, no 6, pp. 2270-2282, Jun. 2016.
5. C.-X. Mao, S. Gao, Y. Wang, Q. Luo, and Q.-X. Chu, “A shared-aperture dual-band dual-polarized filtering-antenna-array with improved frequency response,” IEEE Trans. Antennas Propag., vol. 65, no. 4, pp. 1836–1844, Apr. 2017.
6. S. E. Valavan, D. Tran, A. G. Yarovoy, and A. G. Roederer, “Dual-band wide-angle scanning planar phased array in X/Ku-bands,” IEEE Trans. Antennas Propag., vol. 62, no. 5, pp. 2514–2521, May, 2014.
7. J. A. Kasemodel, C.-C. Chen, and J. L. Volakis, “Wideband planar array with integrated feed and matching network for wide-angle scanning,” IEEE Trans. Antennas Propag., vol. 61, no. 9, pp. 4528–4537, Sep. 2013.
8. L. Zaker, A. Abdipour, A.Tavakoli and R.Mirzavand. Frequency-dependent behavioral-model-based nonlinear analysis and design of a low-profile transmit active phased array antenna. *Int J RF Microw Comput Aided Eng*. 2018;28:e21286.
9. J. Corcoles, M. A. Gonzalez, J. Rubio and J. Zapata, Performance characterization of wideband, wide-angle scan arrays of cavity-backed U-slot microstrip patch antennas. *Int J RF Microw Comput Aided Eng*. 2009;13:e20361.
10. S. M. Moon, S. Yun, I. B. Yom, and H. L. Lee, “Phased Array Shaped-Beam Satellite Antenna With Boosted-Beam Control,” IEEE Trans. Antennas Propag., vol. 67, no. 12, pp. 7633–7636, Jul. 2019.
11. Y. B. Jung and S. Y. Eom, “Dual-Band Horn Array Design Using a Helical Exciter for Mobile Satellite Communication Terminals,” IEEE Trans. Antennas Propag., vol. 60, no. 3, pp. 1336–1342, Mar. 2012.
12. ECC Report-152, “The use of frequency bands 17.3-20.2GHz and 27.5-30.0 GHz by satellite networks,” Gothenburg, September 2010.
13. B. Palacin, et al., “Multibeam Antennas for Very High Throughput Satellites in Europe: Technologies and Trends,” Proc. EuCAP 2017, Paris, France, pp. 2413-2417, May. 2017.
14. U. Tucholke, F. Arndt, T. Wriedt, “Field Theory Design of Square Waveguide Iris Polarizers,” IEEE Transactions on Microwave Theory and Techniques, Vol. 34, pp. 156-160, 1986.
15. A. Bøifot, E. Lier, and T. Schaug-Pettersen, “Simple and broadband orthomode transducer,” IEE Proc. H—Microw. Antennas Propag., vol. 137, no. 6, pp. 396–400, 1990.
16. F. Teberio, I. Arregui, P.Soto, M. A. G. Laso, V. E. Boria and M. Guglielmi, “High-Performance Compact Diplexers for Ku/K-Band Satellite Applications,” IEEE Trans. on microwave theory and techniques, vol. 65, no. 10, pp. 3866-3876, 2017.
17. D. M. Pozar and S. D. Targonski, “A Shared Aperture Dual-Band Dual-Polarized Microstrip Array,” IEEE Trans. Antennas Propag., vol. 49, no. 2, pp. 150-157, Feb, 2001.
18. Y.-R. Ding, Y.-J. Cheng, “Ku/Ka Dual-Band Dual-Polarized Shared-Aperture Beam-Scanning Antenna Array With High Isolation,” IEEE Trans. Antennas Propag., vol. 67, no. 4, pp. 2413–2422, Apr, 2019.
19. F. Qin et al., “A simple low-cost shared-aperture dual-band dual-polarized high-gain antenna for synthetic aperture radars,” IEEE Trans. Antennas Propag., vol. 64, no. 7, pp. 2914–2922, Jul. 2016.